Research Article | Vol. 25, No. 1 | 9 Jan 2017 | OPTICS EXPRESS 39

Optics EXPRESS

Real-time kinetic binding studies at attomolar concentrations in solution phase using a single-stage opto-biosensing platform based upon infrared surface plasmons

T. ALLSOP,[1,*] C. MOU,[2] R. NEAL,[3] S. MARIANI,[4] D. NAGEL,[5] S. TOMBELLI,[6] A. POOLE,[5] K. KALLI,[7] A. HINE,[5] D. J. WEBB,[1] P. CULVERHOUSE,[3] M. MASCINI,[4] M. MINUNNI,[4] AND I. BENNION[1]

[1]*Aston Institute of Photonic Technologies, Aston University, Aston Triangle, Birmingham B47ET, UK*
[2]*Key Laboratory of Special Fiber Optics and Optical Access Network, Shanghai University, Shanghai 200072, China*
[3]*Dept of Maths and Computing, Faculty of Science and Technology, University of Plymouth, Plymouth PL4 8AA, UK*
[4]*Dipartimento di Chimica "Ugo Schiff" and CSGI, Università degli Studi di Firenze, Via della Lastruccia 3, 50019 Sesto Fiorentino, Italy*
[5]*School of Life and Health Sciences, Aston University, Aston Triangle, Birmingham B47ET, UK*
[6]*Istituto di Fisica Applicata Nello Carrara, CNR Via Madonna del Piano 10, 50126 Sesto Fiorentino, Italy*
[7]*Nanophotonics Research Laboratory, Department of Electrical Engineering, Computer Engineering and Informatics, Cyprus University of Technology, 31 Archbishop Kyprianos, Lemessos 3036, Cyprus*
**t.d.p.allsop@aston.ac.uk*

Abstract: Here we present a new generic opto-bio-sensing platform combining immobilised aptamers on an infrared plasmonic sensing device generated by nano-structured thin film that demonstrates amongst the highest index spectral sensitivities of any optical fibre sensor yielding on average 3.4×10^4 nm/RIU in the aqueous index regime (with a figure of merit of 330) This offers a single stage, solution phase, atto-molar detection capability, whilst delivering real-time data for kinetic studies in water-based chemistry. The sensing platform is based upon optical fibre and has the potential to be multiplexed and used in remote sensing applications. As an example of the highly versatile capabilities of aptamer based detection using our platform, purified thrombin is detected down to 50 attomolar concentration using a volume of $1mm^3$ of solution without the use of any form of enhancement technique. Moreover, the device can detect nanomolar levels of thrombin in a flow cell, in the presence of 4.5% w/v albumin solution. These results are important, covering all concentrations in the human thrombin generation curve, including the problematic initial phase. Finally, selectivity is confirmed using complementary and non-complementary DNA sequences that yield performances similar to those obtained with thrombin.

OCIS codes: (240.6680) Surface plasmons; (060.2370) Fiber optics sensors; (220.4241) Nanostructure fabrication; (280.4788) Optical sensing and sensors; (280.1415) Biological sensing and sensors.

References and links

1. A. D. Ellington and J. W. Szostak, "In vitro Selection of RNA Molecules that Bind Specific Ligands," Nature **346**(6287), 818–822 (1990).
2. G. Szakács, J. K. Paterson, J. A. Ludwig, C. Booth-Genthe, and M. M. Gottesman, "Targeting multidrug resistance in cancer," Nat. Rev. Drug Discov. **5**(3), 219–234 (2006).
3. R. Stoltenburg, C. Reinemann, and B. Strehlitz, "SELEX--a (r)evolutionary method to generate high-affinity nucleic acid ligands," Biomol. Eng. **24**(4), 381–403 (2007).
4. S. D. Jayasena, "Aptamers: an Emerging Class of Molecules that Rival Antibodies in Diagnostics," Clin. Chem. **45**(9), 1628–1650 (1999).

#278987 http://dx.doi.org/10.1364/OE.25.000039
Journal © 2017 Received 18 Oct 2016; revised 9 Dec 2016; accepted 11 Dec 2016; published 3 Jan 2017
Corrected: 9 January 2017

Optics EXPRESS

5. X. Ni, M. Castanares, A. Mukherjee, and S. E. Lupold, "Nucleic acid aptamers: clinical applications and promising new horizons," Curr. Med. Chem. **18**(27), 4206–4214 (2011).
6. J. Zhou and J. J. Rossi, "Cell-Specific Aptamer-Mediated Targeted Drug Delivery," Oligonucleotides **21**(1), 1–10 (2011).
7. J. T. B. Crawley, S. Zanardelli, C. K. N. Chion, and D. A. Lane, "The central role of thrombin in hemostasis," J. Thromb. Haemost. **5**(1 Suppl 1), 95–101 (2007).
8. R. F. Macaya, P. Schultze, F. W. Smith, J. A. Roe, and J. Feigon, "Thrombin-binding DNA aptamer forms a unimolecular quadruplex structure in solution," Proc. Natl. Acad. Sci. U.S.A. **90**(8), 3745–3749 (1993).
9. S. R. Garden, G. J. Doellgast, K. S. Killham, and N. J. Strachan, "A fluorescent coagulation assay for thrombin using a fibre optic evanescent wave sensor," Biosens. Bioelectron. **19**(7), 737–740 (2004).
10. A. Leung, P. Shankar, and R. Mutharasan, "A review of fiber-optic biosensors," Sens. Actuators B Chem. **125**(2), 688–703 (2007).
11. T Allsop, R. Neal, S. Rehman, C. Zhang, D. J. Webb, D. Mapps and I. Bennion, "Surface Plasmon Resonance Generation Utilising Gratings for Biochemical Sensing," OFS-18 Cancun Mexico. **WA4**, (2006).
12. T. M. Battaglia, J.-F. Masson, M. R. Sierks, S. P. Beaudoin, J. Rogers, K. N. Foster, G. A. Holloway, and K. S. Booksh, "Quantification of cytokines involved in wound healing using surface plasmon resonance," Anal. Chem. **77**(21), 7016–7023 (2005).
13. S. Patskovsky, A. V. Kabashin, M. Meunier, and J. H. Luong, "Properties and sensing characteristics of surface-plasmon resonance in infrared light," J. Opt. Soc. Am. A **20**(8), 1644–1650 (2003).
14. M. Piliarik, J. Homola, Z. Maníková, and J. Ctyroký, "Surface plasmon resonance sensor based on a single-mode polarisation-maintaining optical fiber," Sens. Actuators B Chem. **90**(1-3), 236–242 (2003).
15. R. Slavík and J. Homola, "Ultrahigh resolution long range surface plasmon-based sensor," Sens. Actuators B Chem. **123**(1), 10–12 (2007).
16. A. J. Haes and R. P. Van Duyne, "A unified view of propagating and localized surface plasmon resonance biosensors," Anal. Bioanal. Chem. **379**(7-8), 920–930 (2004).
17. J. M. Brockman, B. P. Nelson, and R. M. Corn, "Surface Plasmon Resonance Imaging Measurements of Ultrathin Organic Films," Annu. Rev. Phys. Chem. **51**(1), 41–63 (2000).
18. A. G. Brolo, R. Gordon, B. Leathem, and K. L. Kavanagh, "Surface plasmon sensor based on the enhanced light transmission through arrays of nanoholes in gold films," Langmuir **20**(12), 4813–4815 (2004).
19. L. M. Zanoli, R. D'Agata, and G. Spoto, "Functionalized gold nanoparticles for ultrasensitive DNA detection," Anal. Bioanal. Chem. **402**(5), 1759–1771 (2012).
20. S. Tombelli, M. Minunni, and M. Mascini, "A surface plasmon resonance biosensor for the determination of the affinity of drugs for nucleic acids," Anal. Lett. **35**(4), 599–613 (2002).
21. E. J. Cho, J.-W. Lee, and A. D. Ellington, "Applications of Aptamers as Sensors," Ann. Rev. Anal. Chem. **2**(1), 241–264 (2009).
22. G. Spoto and M. Minunni, "Surface Plasmon Resonance Imaging: What Next?" J. Phys. Chem. Lett. **3**(18), 2682–2691 (2012).
23. X. D. Hoa, A. G. Kirk, and M. Tabrizian, "Towards integrated and sensitive surface plasmon resonance biosensors: a review of recent progress," Biosens. Bioelectron. **23**(2), 151–160 (2007).
24. T. Allsop, R. Neal, C. Mou, P. Brown, S. Saied, S. Rehman, K. Kalli, D. J. Webb, J. Sullivan, D. Mapps, and I. Bennion, "Exploitation of multilayer coatings for infrared surface plasmon resonance fiber sensors," Appl. Opt. **48**(2), 276–286 (2009).
25. B. Lee, S. Roh, and J. Park, "Current status of micro- and nano-structured optical fiber sensors," Opt. Fiber Technol. **15**(3), 209–221 (2009).
26. M. J. Kwon, J. Lee, A. W. Wark, and H. J. Lee, "Nanoparticle-enhanced surface plasmon resonance detection of proteins at attomolar concentrations: comparing different nanoparticle shapes and sizes," Anal. Chem. **84**(3), 1702–1707 (2012).
27. T. Allsop, R. Neal, C. Mou, K. Kalli, S. Saied, S. Rehman, D. J. Webb, P. F. Culverhouse, J. L. Sullivan, and I. Bennion, "Formation and characterisation of ultra-sensitive surface plasmon resonance sensor based upon a nano-scale corrugated multi-layered coated D-shaped optical fibre," Quantum Electron. **48**(3), 394–405 (2012).
28. A. M. Bronstein and R. Kimmel, *Numerical Geometry of Non-Rigid Shapes* (Springer Science & Business Media, 2008).
29. C. K. Ho, A. Robinson, D. R. Miller, and M. J. Davis, "Overview of Sensors and Needs for Environmental Monitoring," Sensors (Basel) **5**(1), 4–37 (2005).
30. R. D'Agata and G. Spoto, "Surface plasmon resonance imaging for nucleic acid detection," Anal. Bioanal. Chem. **405**(2-3), 573–584 (2013).
31. T. W. Ebbesen, H. J. Lezec, H. F. Ghaemi, T. Thio, and P. A. Wolff, "Extraordinary optical transmission through sub-wavelength hole arrays," Nature **391**(6668), 667–669 (1998).
32. A. Kolomenski, A. Kolomenskii, J. Noel, S. Peng, and H. Schuessler, "Propagation length of surface plasmons in a metal film with roughness," Appl. Opt. **48**(30), 5683–5691 (2009).
33. J. Hu, X. Sun, A. Agarwal, and L. C. Kimerling, "Design guidelines for optical resonator biochemical sensors," JOSAB **26**(5), 1032–1041 (2009).
34. T. Allsop, R. Neal, C. Mou, P. Brown, S. Saied, S. Rehman, K. Kalli, D. J. Webb, J. Sullivan, D. Mapps, and I. Bennion, "Exploitation of multilayer coatings for infrared surface plasmon resonance fiber sensors," Appl. Opt. **48**(2), 276–286 (2009).

Optics EXPRESS

35. B. Lee, S. Roh, and J. Park, "Current status of micro- and nano-structured optical fiber sensors," Opt. Fiber Technol. **15**(3), 209–221 (2009).
36. X. D. Hoa, A. G. Kirk, and M. Tabrizian, "Towards integrated and sensitive surface plasmon resonance biosensors: a review of recent progress," Biosens. Bioelectron. **23**(2), 151–160 (2007).
37. A. D. Attie and R. T. Raines, "Analysis of Receptor-Ligand Interactions," J. Chem. Educ. **72**(2), 119–123 (1995).
38. B. Alexander, D. J. Browse, S. J. Reading, and I. S. Benjamin, "A simple and accurate mathematical method for calculation of the EC_{50}.," J. Pharmacol. Toxicol. Methods **41**(2-3), 55–58 (1999).
39. J. Homola, "Surface Plasmon Resonance Sensors for Detection of Chemical and Biological Species," Chem. Rev. **108**(2), 462–493 (2008).
40. T. Tumolo, L. Angnes, and M. S. Baptista, "Determination of the refractive index increment (*dn/dc*) of molecule and macromolecule solutions by surface plasmon resonance," Anal. Biochem. **333**(2), 273–279 (2004).
41. M. L. Ermini, S. Mariani, S. Scarano, and M. Minunni, "Direct detection of genomic DNA by surface plasmon resonance imaging: an optimized approach," Biosens. Bioelectron. **40**(1), 193–199 (2013).
42. J. Go and M. A. Alam, "Statistical interpretation of "femtomolar" detection," Appl. Phys. Lett. **95**(3), 033110 (2009).
43. P. R. Nair and M. A. Alam, "Performance limits of nanobiosensors," Appl. Phys. Lett. **88**(23), 233120 (2006).
44. P. E. Sheehan and L. J. Whitman, "Detection Limits for Nanoscale Biosensors," Nano Lett. **5**(4), 803–807 (2005).
45. A. Hassibi, H. Vikalo, and A. Hajimiri, "On noise processes and limits of performance in biosensors," J. Appl. Phys. **102**(1), 014909 (2007).
46. X. Fan, I. M. White, S. I. Shopova, H. Zhu, J. D. Suter, and Y. Sun, "Sensitive optical biosensors for unlabeled targets: a review," Anal. Chim. Acta **620**(1-2), 8–26 (2008).
47. A. Pinto, M. C. Bermudo Redondo, V. C. Ozalp, and C. K. O'Sullivan, "Real-time apta-PCR for 20 000-fold improvement in detection limit," Mol. Biosyst. **5**(5), 548–553 (2009).
48. B. Strehlitz, N. Nikolaus, and R. Stoltenburg, "Protein Detection with Aptamer Biosensors," Sensors (Basel) **8**(7), 4296–4307 (2008).
49. X. Fan and I. M. White, "Optofluidic microsystems for chemical and biological analysis," Nat. Photonics **5**(10), 591–597 (2011).
50. L. Gaspari, F. Paris, P. Philibert, F. Audran, M. Orsini, N. Servant, L. Maïmoun, N. Kalfa, and C. Sultan, "'Idiopathic' partial androgen insensitivity syndrome in 28 newborn and infant males: impact of prenatal exposure to environmental endocrine disruptor chemicals?" Eur. J. Endocrinol. **165**(4), 579–587 (2011).
51. M. Ninivaggi, R. Apitz-Castro, Y. Dargaud, B. de Laat, H. C. Hemker, and T. Lindhout, "Whole-Blood Thrombin Generation Monitored with a Calibrated Automated Thrombogram-Based Assay," Clin. Chem. **58**(8), 1252–1259 (2012).
52. J. J. van Veen, A. Gatt, and M. Makris, "Thrombin generation testing in routine clinical practice: are we there yet?" Br. J. Haematol. **142**(6), 889–903 (2008).
53. H. C. Hemker, R. Al Dieri, E. De Smedt, and S. Béguin, "Thrombin generation, a function test of the haemostatic-thrombotic system," Thromb. Haemost. **96**(5), 553–561 (2006).
54. Z. Fang, L. Soleymani, G. Pampalakis, M. Yoshimoto, J. A. Squire, E. H. Sargent, and S. O. Kelley, "Direct Profiling of Cancer Biomarkers in Tumor Tissue Using a Multiplexed Nanostructured Microelectrode Integrated Circuit," ACS Nano **3**(10), 3207–3213 (2009).
55. http://www.rockefeller.edu/spectroscopy/instruments_spr
56. S. Centi, G. Messina, S. Tombelli, I. Palchetti, and M. Mascini, "Different approaches for the detection of thrombin by an electrochemical aptamer-based assay coupled to magnetic beads," Biosens. Bioelectron. **23**(11), 1602–1609 (2008).
57. W. Potze, E. M. Alkozai, J. Adelmeijer, R. J. Porte, and T. Lisman, "Hypercoagulability following major partial liver resection - detected by thrombomodulin-modified thrombin generation testing," Aliment. Pharmacol. Ther. **41**(2), 189–198 (2015).

1. Introduction

Progress in biotechnology demands sensing platforms that can be readily combined with the specific and selective binding of target molecules by the inclusion of affinity reagents, such as aptamers, antibodies and other antibody mimetics. Aptamers (specific, single-stranded DNA oligonucleotides) are attractive affinity reagents and are potential antibody replacements for the development of biomolecular nanosensors owing to their high affinity, specificity, in-vitro synthesis and stability [1, 2]. Aptamers are analogous to antibodies with respect to the variety of substances they can detect and their range of applications, but they have some distinct advantages [3]. One is their greater specificity and affinity [4], while others include their ability to tolerate a larger range of pH environments and temperature variations [3], with aptamers being more stable than antibodies. Moreover, aptamers have a

Optics EXPRESS

greater shelf life than antibodies. The development of nucleic acid based aptamers and research into their potential applications has gathered pace since their inception in 1990 [1]. These single-stranded short oligonucleotides form three-dimensional structures that bind to their target molecule with high affinity and specificity. As the oligonucleotides are short (15-60 bp) they can be routinely and reproducibly synthesised chemically. The development of aptamers with affinity for a diverse range of biological targets has led to their employment not only in diagnostics but also in clinical/therapeutic [5] applications and as the affinity reagents in cell specific drug delivery [6].

Of particular interest is the serine protease thrombin, which is crucial to clot formation and the blood coagulation process and is also important in anticoagulation, wound healing, chemotaxis and inflammatory responses [7]. Due to its important and diverse biological roles, thrombin was one of the initial targets for aptamer development [8]. As such, a wealth of literature characterizes not only the thrombin aptamer interaction, but also the use of such aptamers in thrombin quantification. Fibre optic evanescent wave sensors based upon fluorescent coagulation [9] and surface plasmon resonance (SPR) sensors [10–12], have been developed recently. These have been used to detect other biochemical compounds by utilising immobilized bio-recognition molecular coatings on a metallic surface.

SPR is an important optical phenomenon that involves the resonant transfer of incident propagating light to surface-plasmon modes that take the form of collective electron oscillations in a metal [13]. Sensors exploiting SPR can be divided into three types based upon the kind of surface plasmon being generated at the metal/dielectric interface: long range surface plasmons (LRSP) [14], short range surface plasmons (SRSP) [15] and localised surface plasmons (LSP) [16]. SPR biosensors offer the opportunity for real-time and label-free monitoring of biomolecular interactions [17]. The plasmons exist at a metal–dielectric interface and depending on the topology of the supporting metal coating the dispersion relation can change [16]; the LRSP and SRSP obey the same dispersion relationship, whereas localised surface plasmons have a strong dependence on the surface structure [18].

We have previously reported some initial, modest experimental results of plasmonic fibre sensors [11] working in conjunction with aptamers that have shown potential as an optical chemical sensing platform. . SPR-based DNA sensing has previously achieved sensitivities down to femto and even atto-molar concentrations utilising enhancement amplification techniques [19–21], however these enhancement techniques at best complicate the binding mechanism with the inclusion of additional particles [22] and thus modify and compromise the binding kinetics.

The authors here report for the first time an optical biosensing platform working with an immobilised aptamer that is able to detect attomolar concentrations of thrombin directly, without any further enhancement techniques (in a sample volume of $1mm^3$). The foundation upon which these results are based is an optical sensing platform utilizing surface plasmons resonances and offering spectral sensitivity to refractive index in excess of 3.4×104 nm/ RIU, leading to a conservative detection limit of 2.0×10^{-6} with a F.O.M. of 330 in the aqueous index regime for the sensing platform. This spectral index sensitivity is the highest reported in the literature [23–25] and leads to one of the highest index resolutions [23–25]. This result not only represents a 2 to 3 orders of magnitude improvement in detection limit over previous reports [26], but is also in the same range as those employing additional enhancement amplification techniques. The experimental data presented in this paper show the system is capable of monitoring in the solution phase and in real-time the binding of the aptamer to the target molecule without any additional species being involved, giving experimentalists the opportunity to study binding kinetics without the added complexity of an enhancement technique

Optics EXPRESS

2. Fabrication and characterisation of bio-sensing platform

2.1 Optical sensing platform fabrication

For ease of interrogation an optical fibre platform was used for the devices, as has previously been described [27]. The devices were processed in three stages, resulting in a D-shaped fibre with nano-structured multi-layered coatings. The multi-layered coatings consisted of three different materials: germanium (48nm), silicon dioxide (48nm) and gold (38nm). The nano-structuring consisted of surface corrugations with dominant structured spatial periods close to 0.5μm, 1μm, 2μm and 4μm, see schematic Fig. 1(a) and 1(b).

In brief, a lapped region of the fibre is coated sequentially with three materials; firstly germanium is deposited upon the lapped fibre followed by silicon dioxide and finally gold (Au-SiO_2-Ge/fibre). The nano-structuring of this coating is created by utilising the photobleaching effect that UV laser light has on germanium oxides, found in the multi-layered coating; the UV light produces a change in the optical properties (refractive index) and generates material compaction (a geometrical structural change [27]). This second effect is used to generate the nano-structure (array of nano-wires) of the coating. The UV irradiance pattern is generated by a phase mask, producing a diffraction pattern that is conventionally used to produce fibre Bragg gratings. The UV irradiance is produced using an argon ion laser (Innova® Sabre® FRED) operating at 244nm.

Typical fabrication parameters used are a scanning velocity of 0.05mms^{-1} and a UV optical power on the fibre itself of approximately 120mW. The equipment and alignment used for producing conventional fibre Bragg gratings is used to create the nanostructured coated D-shaped fibres. A typical period of a phase mask used in this process is 1.072 μm and a typical surface topology created by this procedure is shown in Fig. 1(c) along with a schematic of the sensing evanescent field. The surface topologies have been characterised physically and chemically using an atomic force microscope (Park Scientific Instruments AutoProbe, Thermomicroscopes) (AFM) and X-ray Photoelectron Spectroscopy, (Thermo Fisher ESCALAB 250 Imaging XPS Instrument, spatial resolution 10nm) XPS. It was found that the resultant surface topology was characterised by regions having corrugation and the XPS revealed that the apexes of the surface ridges were metal surrounded by dielectric material. This creates an array of parallel nanowires perpendicular to the central axis of the optical fibre, see Figs. 1(c) and 1(d). The total length of the array depends upon the lapped region of the fibre, the length of the phase mask used and the scanning length of UV irradiance; typically the total length of the array is approximately 2.2cm. The nominal dimensions of a single corrugation are as follows: approximate length 20 μm (perpendicular to the optical fibre central axis), with the individual apex of the corrugation having an average FWHM 180nm ± 20 nm. Figure 1(e), shows a cross-section line profile for a few corrugations. Furthermore, closer inspection of Fig. 1(c) shows the UV processed region and pristine areas that are flat. Performing a Fast Fourier Transform on the AFM scan showed we have various spatial periods present with the predominant period being approximately half the phase mask period. The particular example yields periods of 0.348μm, 0.512μm and 1.087μm, see Fig. 1(f). A higher resolution AFM scan revealed fine surface structures within a single nano-antenna, this appears to be due to the fact the phase mask produces a 3-dimensional interference pattern, see Fig. 1(d). These arrays support localised surface plasmons [27].

Optics EXPRESS

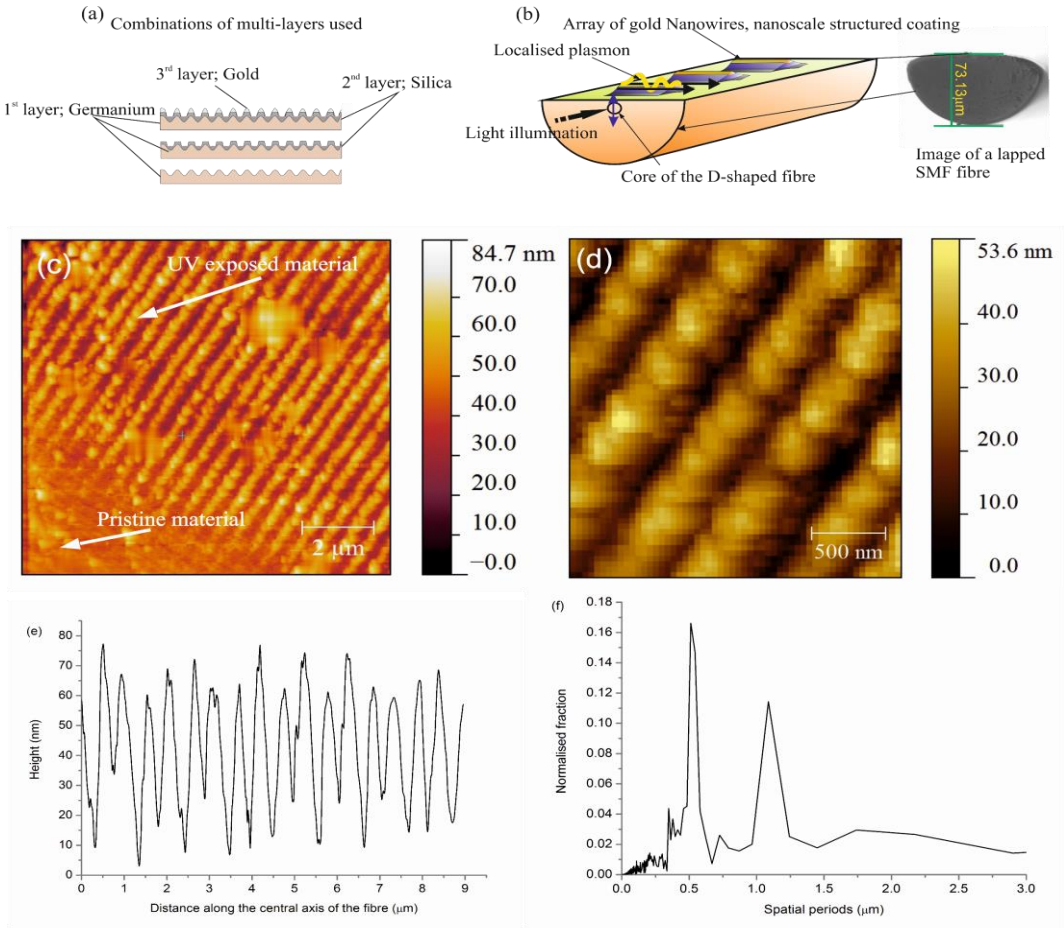

Fig. 1. (a) Schematic representation of the multi-layered and nanoscale structured coating that supports the localised surface plasmons (b) Representation of the structured thin film coating created after the various stages of processing. (c) An example of an AFM image of the sensing region on the flat of the D-shaped fibre showing the surface corrugation after UV processing and a pristine surface. (d) An example of AFM image showing the fine structure within several nano-antennas. (e) Typical experimental data of the height variation across several nano-antennas. (f) A typical FFT of the cross-section along the nano-antenna array that is along the optical fibre axis and perpendicular to a single nano-antenna.

The devices were characterised by measuring changes in their response as a function of the azimuthal polarisation properties of the illuminating light and of the surrounding medium's refractive index. For the latter experiments, the fibres were placed in a V-groove and immersed in certified refractive index liquids that have a quoted accuracy of ± 0.0002, Fig. 2(a). The V-groove was made in an aluminium plate, machined flat to minimise bending of the fibre. The plate was placed on an optical table, which acted as a heat sink to help maintain a constant temperature throughout the experiments.

2.2 Optical detection scheme

Light from a broadband light source, was passed through a polariser and a polarisation controller before illuminating the sample, with the transmission spectrum being monitored using an optical spectrum analyser. The change in polarisation of the illuminating light was monitored with a polarimeter (Tektronix, PAT 9000B) through a polarisation maintaining

Optics EXPRESS

coupler, see Fig. 2(a). Due to the spectral broadness of the surface plasmon transmission features that are used to measure the concentration changes, the central wavelengths were calculated by using the first moment of the power spectrums; i.e. the centroid by geometric decomposition [28]. The associated transmission centroid strength value of the SPR was obtained as the mean value over the range where the extinction transmission feature is greater than 6dB level in attenuation.

2.3 Aptamer thrombin assay procedure

Prepared fibres were coated with a thrombin aptamer 5′ – SH(CH2)6 - GGT TGG TGT GGT TGG - 3′ [29, 30]. The aptamer was immobilised to the fibre by a thiol mediated linkage. Fibres were stored in potassium phosphate buffer (100mM pH7.4). Alpha thrombin from human plasma was obtained from Sigma (Sigma T6884). Binding buffer (50mM Tris 140mM NaCl 1mM MgCl2) pH 7.4, was used for all binding experiments. The BSA was supplied by Sigma-Aldrich product A9418.

2.4. Detection of thrombin

Thrombin solutions ranging from concentrations of 5aM to 1μM were prepared in a binding buffer by performing serial logarithmic dilutions on ice (to prevent de-naturation of the thrombin). The sensor was used in two different experiments; firstly, using a fixed volume of solution of thrombin, the sensor being exposed to the solutions lying in a flat aluminium v-groove. After each thrombin solution was used the v-groove and the sensors were washed in a 4 molar solution of NaCl to regenerate the sensors and further washed in 50 mM Tris binding buffer solution (pH 7.4). The apparatus used in these experiments are shown Fig. 1(a). The second experiment used a flow sample cell attached to a syringe driver to deliver a constant flow rate of a given solution, Fig. 2(b). Both sets of experiments consisted of two separate tests. The first was the detection of various concentrations of thrombin dissolved in buffer solution (50 mM Tris 140 mM NaCl 1 mM MgCl2) pH 7.4, using both a fixed volume and a flow sample cell used with a flow rate of 5 μl/min. The second involved a repeat of these same experiments with the same concentrations of thrombin but in bovine serum albumin (BSA) at a concentration of 4.5% w/v, dissolved in a 50 mM Tris buffer solution (pH 7.4), which provides very similar test condition to samples from human beings.

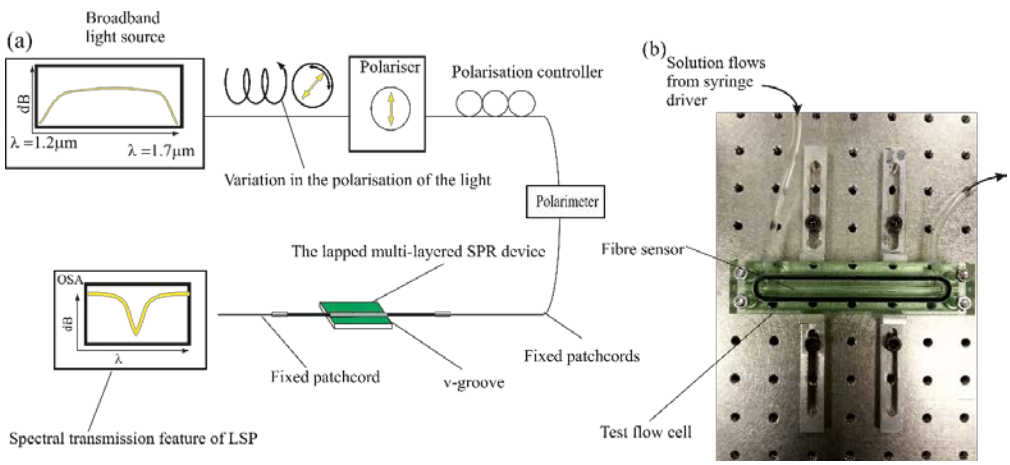

Fig. 2. Scheme used for the characterisation of the devices and the detection of the thrombin in ultra-low concentration solutions, (a) schematic of experimental apparatus used for fixed volumes of thrombin solutions and equipment to optimise the polarisation of the illuminating light to obtain a LSP resonance with maximum optical strength in the transmission spectra, (b) image of the sample cell used for constant solution flow experiments.

Optics EXPRESS

3. Experimental results for optical sensing platform and biosensor

3.1 Optical sensing platform spectral behavior and performance

After the bare fibres are lapped, their spectral index and polarisation sensitivities are measured to ensure that the core of the fibre is not exposed and that there is enough optical dynamic range,so that the surface plasmon resonances in transmission can be fully measured. The highest refractive index solution used on the bare fibres is 1.448, because this is approximately the refractive index of the cladding, thus effectively removing the cladding/surrounding medium interface. Figures 3(a)-3(b) show a typical spectral index response and sensitivity of the bare D-shaped fibre. On inspection the individual spectra display a reasonably flat wavelength response with increasing index, up to the highest refractive index (1.448), displaying an average optical power loss of approximately 7 dB from air, with a device loss of ~1.8dB, see Fig. 3(b). The optical power losses as a function of polarisation were also investigated from an initial arbitrary polarisation state, this revealed that the average optical power varied by ± 1 dB, see Fig. 3(c). Furthermore, there appears to be an asymmetric variation in the response to polarisation and this is due to the initial arbitrary starting-point.

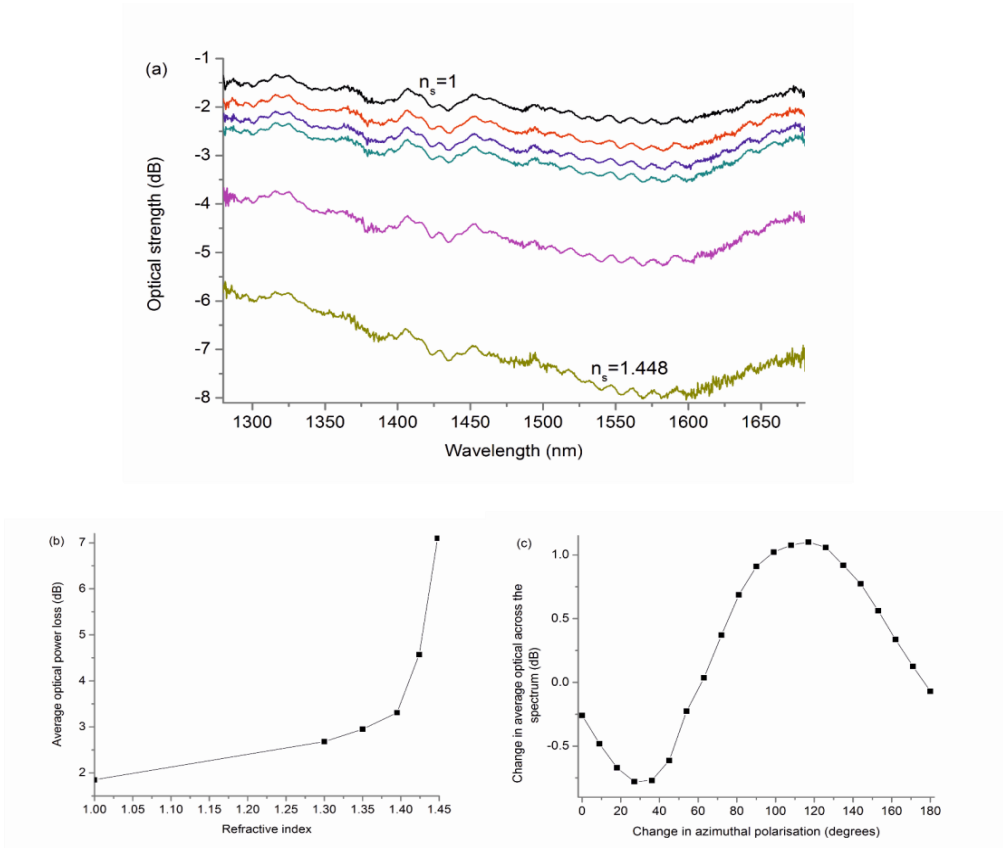

Fig. 3. The spectral characterisation of the bare D-shaped fibre before coating and UV processing (a) the response of transmission spectra with increasing refractive index. (b) The average optical attenuation losses over the spectral range of 1250nm to 1690nm. (c) The variation of the average optical attenuation losses as a function of azimuthal polarisation measured from an initial, arbitrary polarisation state.

After the array of nano-wires is produced on the D-shaped fibres and before the immobilisation of the thrombin aptamer, the spectral characteristics were again investigated

Optics EXPRESS

with regard to changes in the refractive index of the surrounding medium and the light polarisation. A schematic of the apparatus to investigate the spectral behaviour is shown in Fig. 2(a) and described further in the method section. Figure 4(a) and Fig. 4(b) shows the polarisation dependence of these devices and Fig. 5 shows the typical transmission spectral variation with changes in surrounding refractive index.

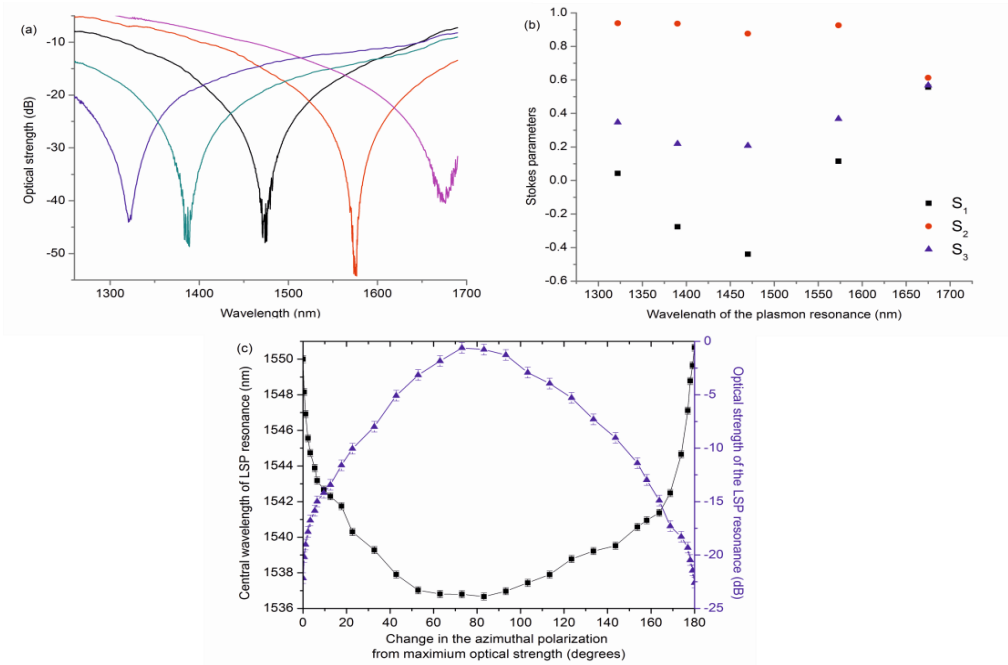

Fig. 4. The polarisation dependence of the optical sensing platform (Au-SiO2-Ge/fibre) before aptamer immobilisation: (a) an example of the spectral dependence upon polarisation (b) The Stokes parameters of the illuminating light of resonances across the spectral range of interest (c) the typical azimuthal polarisation dependence of a localised surface plasmon in air.

Figure 4(a) illustrates that a single device can generate surface plasmon resonances of comparable strength over the available light source wavelength range, using all possible polarisation states of the illuminating light. For completeness of investigation we measured the degree of polarisation of the illuminating light used to produce the series of surface plasmon resonances over the spectral range of interest; 1280nm to 1690nm. The Stokes parameters were measured using an in-line polarimeter (General Photonics, Polarisation Analyser, POD-201) and the results are shown in Fig. 4(b). It was found that the percentage of the "Degree of Polarisation" varied linearly as a function of wavelength from 96.8% to 87.6% from the lower to higher wavelengths, respectively. The greatest variation occurring is with the azimuth of polarisation from 58.3 to 23.5 degrees, this doesn't appear to be linear with spectral location of the resonance. The Stokes parameter S1 implies the light is linearly polarised, with both positive and negative values. These results are showing variations from horizontal to vertical linearly polarisation, which is expected due to the experimental set-up. The Stokes parameter S_2 seems to be varying from 0.7 to 0.9; S_2 is associated with angled linearly polarised and S_3 has positive values which is associated with right-handed circularly polarised light. The S_2 and S_3 parameters are suggesting different surface topological features are associated with the different transmission resonances.

There are several reasons for this spectral tunability: the plasmons exist at a metal–dielectric interface and depending on the topology of the supporting metal coating the

Optics EXPRESS

dispersion relation can change [16]; the LRSP and SRSP obey the following dispersion relation for two homogeneous semi-infinite media:

$$\beta = k\sqrt{\left(\frac{\varepsilon_m \cdot n_s^2}{\varepsilon_m + n_s^2}\right)} \tag{1}$$

where k is the free space wave number, ε_m is the dielectric constant of the metal ($\varepsilon_m = \varepsilon_{mr} + i\,\varepsilon_{mi}$) and n_s is the refractive index of the dielectric sample to be tested. A corrugated nano structure can be considered as an array of apertures [31], with the momentum component of light parallel $k_x = \frac{2\pi}{p}\cdot\sqrt{i^2 + j^2}$ to the surface, where p is a lattice constant (the distance between the apertures), i and j are nonzero integer numbers, representing the scattering orders from the two dimensional aperture arrays. The resonant condition for the localised surface plasmons that needs to be satisfied for a lattice structure is given by [18]. From the FFTs of a typical UV processed surface shown in Fig. 1(c) and Fig. 1(d) there are a few potential lattice constants from primary structure of the nano-wire/nano-antenna array and from an individual nano-antenna.

The tunability is increased by the imperfections in the fabrication process (such as misalignment of the D-shaped fibre, the variations in the focusing of the UV light, variations in the alignment of the phase mask to the fibre and UV light intensity) causing a variation in the nanowires' shapes, size, geometries and composition, which would yield a variation in the phase matching condition for the excitation of resonances and spectrally broaden the resonances and implies short propagation lengths [32], which are observed experimental Furthermore, the spectral features have large tunability and vary in coupling strength as a function of polarization, and this indicates the presence of localized surface plasmons, instead of surface plasmons having short propagation lengths on rough surfaces that would produce reasonable resonance coupling over the azimuthal polarisation range from 0° to 180°. This fact along with the high polarisation sensitivity of 2.7dB/degree at the maximum strength of the excitation resonances shown in Fig. 4(b), indicates that the optical sensing platform is generating localised surface plasmons (LSPR).

Optics EXPRESS

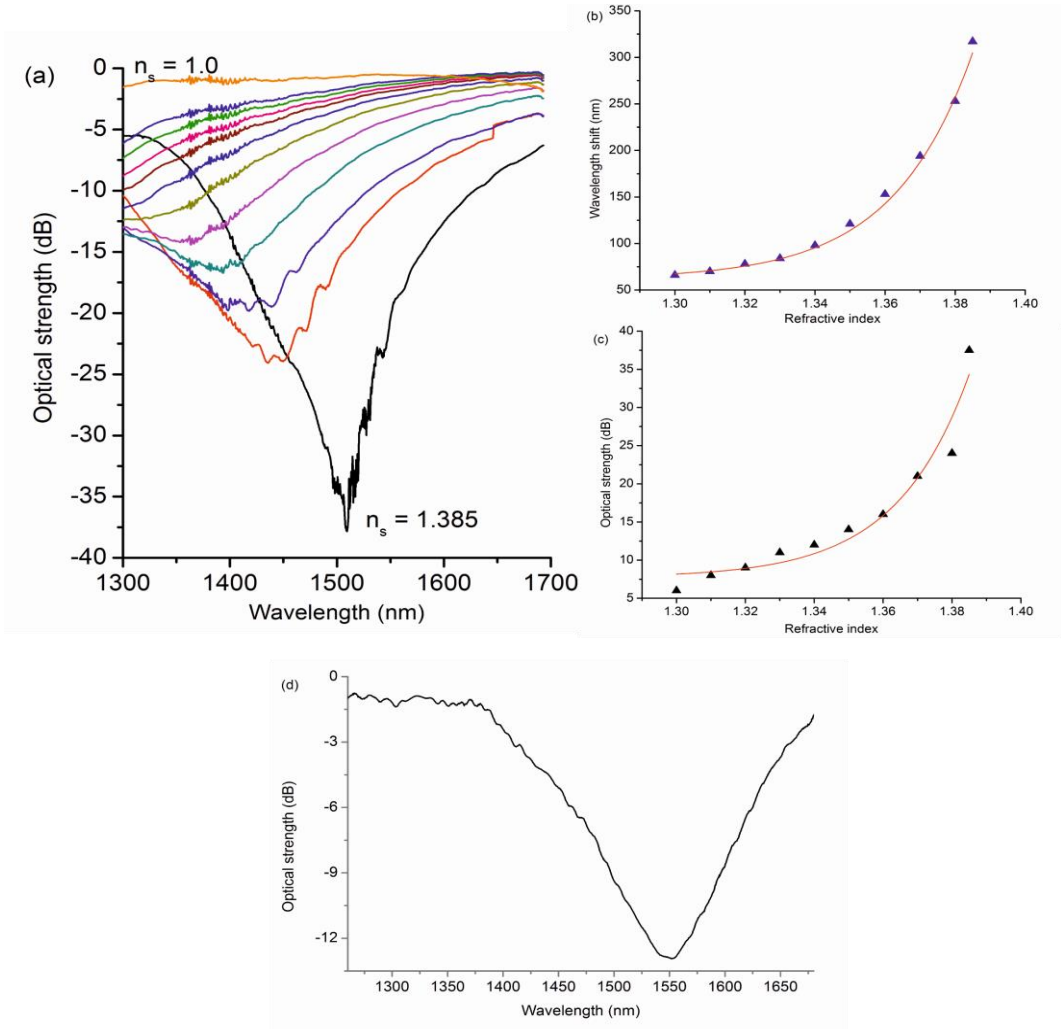

Fig. 5. (a) The spectral transmission characteristics of the device (Au-SiO2-Ge/fibre) as a function of the index of the surrounding medium and (b) the spectral wavelength shift vs index. (c) The optical strength as a function of surrounding refractive index before aptamer immobilisation. (d) The transmission spectrum of the device after immobilisation of the thrombin aptamer when submerged in a buffer solution.

Inspecting the results for the resonance wavelength dependence on surrounding index, Figs. 5(a)-5(d) reveals a maximum bulk refractive index sensitivity of $\Delta\lambda/\Delta n$ of 1.7×10^4 nm/RIU in the aqueous index regime, which yields a refractive index resolution of 5.9×10^{-6} and a Figure-of-Merit (FOM) of 210, determined using a standard approach [10, 17, 33–36] defined as FOM = $(\Delta\lambda/\Delta n)/\Delta\lambda_{FWHM}$, where $\Delta\lambda_{FWHM}$ is the full width at half maximum of the spectral feature. The index resolution is determined in part by the utilized interrogation scheme, which in this case is an optical spectrum analyser (OSA) that has 1000 measurable points over the FWHM of the resonance (80nm), leading to measurable resolution of 0.08nm (greater than the resolution of the OSA). The peak resonance was measured over a 10 minute period yielding a variation of ± 0.1nm. The FOM value for this sensing platform is reasonably good and has a typical mid-range value compared to other sensing systems [10, 17, 33–37]. The optical strength variation produced an index intensity sensitivity of $\Delta I/\Delta n$ =

Optics EXPRESS

2.7×10^{3} and yielded a resolution of 1.0×10^{-4} with a FOM of 97, which is less than was obtained for wavelength interrogation. Whilst the overall index sensitivity is very high the spectral features are relatively broad thus compromising the overall detection limit. The spectral sensitivities quoted above are typical of these devices, but there are variations. The spectral broadness of the surface plasmons and spectral characteristics are a function of the variation of the nanowires' shapes, sizes and geometries, which can be improved and standardised through refining the fabrication technique. Figure 5(d) shows a typical transmission spectrum following immobilisation of the thrombin aptamer on the surface of the device when submerged in buffer solution. It is useful to estimate the index spectral sensitivity of the aptamer coated sensing platform for the reader to make comparisons. To achieve this, without compromising or corrupting the performance of the aptamer coated sensing platform with additional submersions into standard refractive index solutions, we used existing data from before the immobilisation of the thrombin aptamer, in particular the refractive index spectral sensitivity data given in Fig. 5(b) that were obtained at the maximum excitation response for polarisation for each index solution. If we account for the measured maximised excitation of LSPR spectral location and assuming that the spectral sensitivity as a function of index continues with the same behavior at longer wavelengths, shown in Fig. 5(b), it is estimated that the wavelength spectral sensitivity is approximately 3.4×10^{4} nm/ RIU, leading to a conservative detection limit of 2.0×10^{-6} with a F.O.M. of 330 in the aqueous index regime for the sensing platform immobilised with the thrombin aptamer. These results are the highest index spectral sensitivities reported in the literature [23–25] and amongst the highest index resolutions [23–25].

3.2 Detection of thrombin

Thrombin solutions ranging from concentrations of 5 aM to 1 μM were prepared on ice and then examined in two formats. Purified thrombin was first assayed in static buffer solution in the apparatus illustrated in Figs. 1a and 1b, which demonstrated clear detection of thrombin down to 1 nM concentration, Figs. 6(a) and 6(b). Thrombin was also detected within bovine serum albumin (BSA) at a concentration of 4.5% w/v dissolved in a 50 mM Tris buffer solution (pH 7.4), in a flow cell as illustrated in Fig. 2(b)c. In this solution format, which aims to simulate human samples more closely, thrombin was detected at a 100 pM concentration. Moreover, in the flow-cell format, both association and dissociation of thrombin to the aptamer are visualized, Figs. 6(c) and 6(d).

Figure 6(a) shows the overall wavelength shift with a graphical axis break to show the finer detail of the wavelength variation as a result of the various concentrations of thrombin in the 50 mM Tris buffer solution (pH 7.4). Figure 6(b) shows the change in optical strength at the central wavelength of the SPR spectral feature: as the concentrations increase the overall power increases from a baseline of –4.8dB. We note that we neglected to include the initial optical strength of the plasmon resonance due to the fact we wanted to show clearly the changes in optical strength due to the differing concentrations of thrombin. Inspecting Fig. 6(a) it is noticeable that initial injections lead to a significant red-shift owing to the physical effects of mixing, however, once equilibrium has been reached, the greater the concentration of thrombin, the larger the blue-shift of the wavelength. This mixing effect can be seen in the transition period between the solutions with different concentrations. The change in optical strength of the resonance is more distinguishable than the wavelength changes, which prove to be relatively small. However, the latter are absolute measurements, whereas the optical strength can be corrupted by transient attenuation losses, such as fibre bending.

Optics EXPRESS

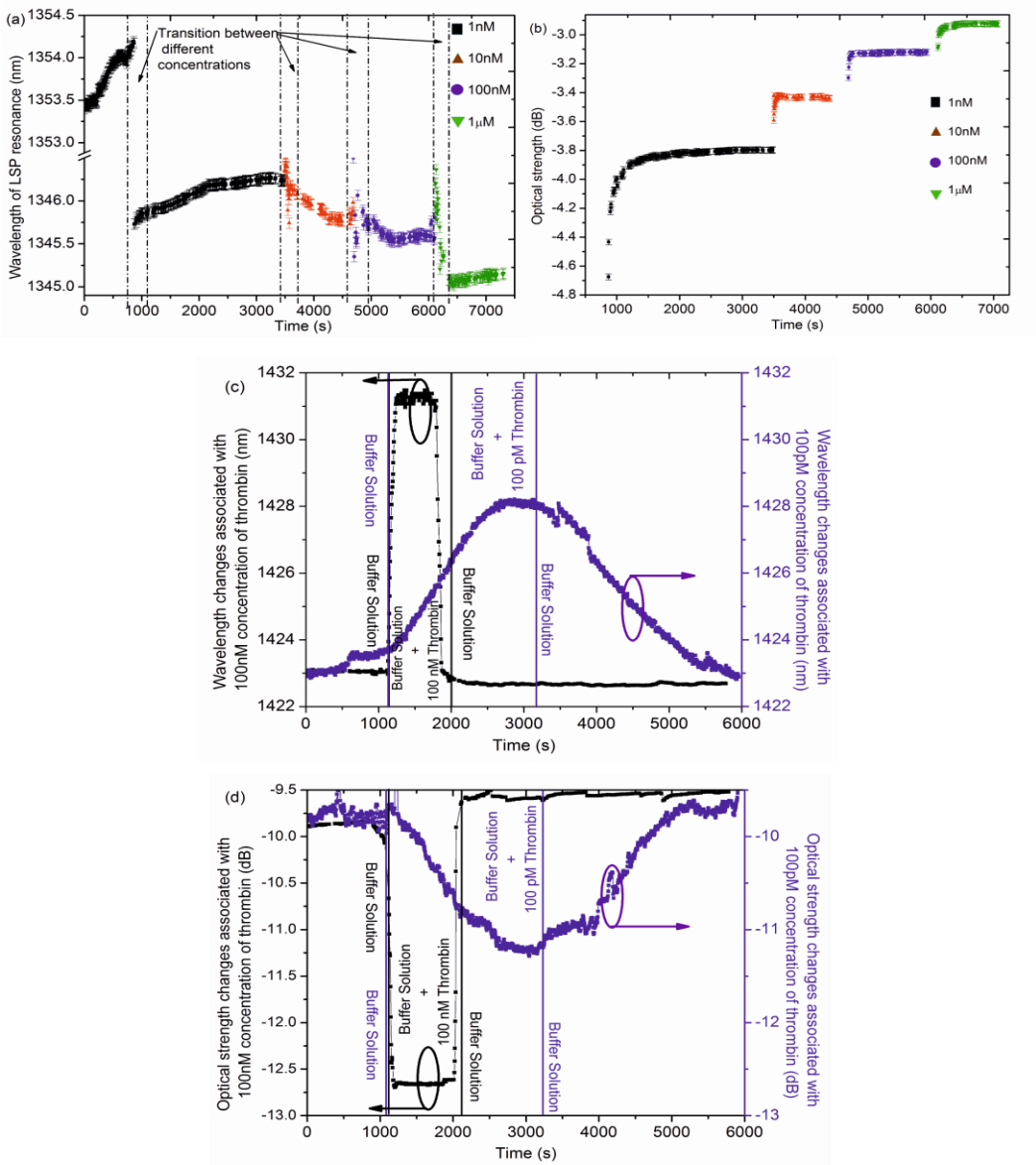

Fig. 6. Performance of the Au-SiO_2-Ge/fibre coated aptamer device in the detection of thrombin. Parts (a) & (b) show wavelength shift and optical strength at the central wavelength responses respectively, in a fixed volume of static buffer, as a function of time, in response to thrombin concentrations over three orders of magnitude (1 nM → 1 μM) where thrombin was introduced at approximately 800 seconds. Parts (c) and (d) show similar results for two concentrations of thrombin in a flow cell with constant flow rate of 5 μl/min, using a Tris Buffer solution with a thrombin concentration of 100 nM (—) and 100 pM (—), with injections of buffer / buffer/thrombin mix as indicated.

Flow experiments were conducted with various concentrations of thrombin using flow rates of 5 μl/min. Figure 6(c) and 6(d) illustrate typical association and dissociation of the thrombin (examples are 100 pM and 100nM) with aptamers immobilised on the surface of the optical sensor.

Optics EXPRESS

We observe that with these devices the LSP resonances are tunable over a very large wavelength range, as shown in Fig. 4(a). This also means the spectral characteristics (i.e. wavelength shift, spectral broadness and optical strength) and spectral sensitivity are very much dependent upon the spectral location of the LSP resonance through the material dependent dispersion characteristics [13, 16, 23]. The dispersion relationship can result in blue or red wavelength shifts as a function of the surrounding refractive index and an increase or decrease in the optical strength of the resonance. This is illustrated in Fig. 6, with Fig. 6(a) and 6(b) having a resonance at a wavelength close to 1353nm and producing blue wavelength shifts with increasing concentration whilst Fig. 6(c) and 6(d) have a resonance near 1423nm and produce a red wavelength shift.

For the range of concentrations used there appears to be a demarcation from conventional equilibrium response with time at concentrations of about 100 pM and below. This can be seen in the association and dissociation time response curves shown in Figs. 6(c) and 6(d) with the lower concentration starting to show an unusual characteristic curve with additional smaller features appearing on the curves and what appears to be increasing variance at the steady state condition for this reaction. This behaviour is further illustrated in Fig. 7, showing the binding time response curve for a concentration of 50 aM.

The detection limit of these devices was then tested with a series of experiments with different sensors exposed to ultra-low concentrations of thrombin in 50 mM Tris buffer solution (pH 7.4) - ranging from 5 aM to 1 pM concentrations in static format (Fig. 1b). A summary of three typical sensors' spectral response to various concentrations of thrombin are shown in Figs. 7(a) and 7(b). Meanwhile, the time response of one of the devices at one of the lower concentrations (50 aM) is shown in Figs. 7(c) and 7(d).

These three typical fibre devices were employed to take measurements over the concentration range. There appears to be a log-linear relationship between thrombin concentration and both wavelength shift and change in optical strength Figs. 7(a) and 7(b), albeit that the correlation is closest between thrombin concentration and change in optical strength. These data sets demonstrate consistent behaviour of this sensing platform. Interestingly, the response times (estimated to be the time taken for the trend of the response of the system to settle) of these equilibriums for different concentration solutions do not have a linear relationship with concentration, Fig. 7(e). Closer inspection of Fig. 7(e) shows that at approximately 100 pico-molar concentration there seems to be a change in the relationship of settling/incubation time to concentration; which is further explored in the discussion. However, the change in wavelength demonstrates greater resolution over the log-linear range inasmuch as the response to attomolar solutions is clearly visible in terms of wavelength shift, Fig. 7(a), but barely discernable in terms of change in optical strength, Fig. 7(b). Nevertheless, by adjusting the scale, binding between 50 aM thrombin and the immobilised aptamer is detectable by either measurement method, Figs. 7(c) and 7(d). This is particularly notable, since a concentration of 50 aM is equivalent to approximately 30 molecules of thrombin per µl of solution.

Optics EXPRESS

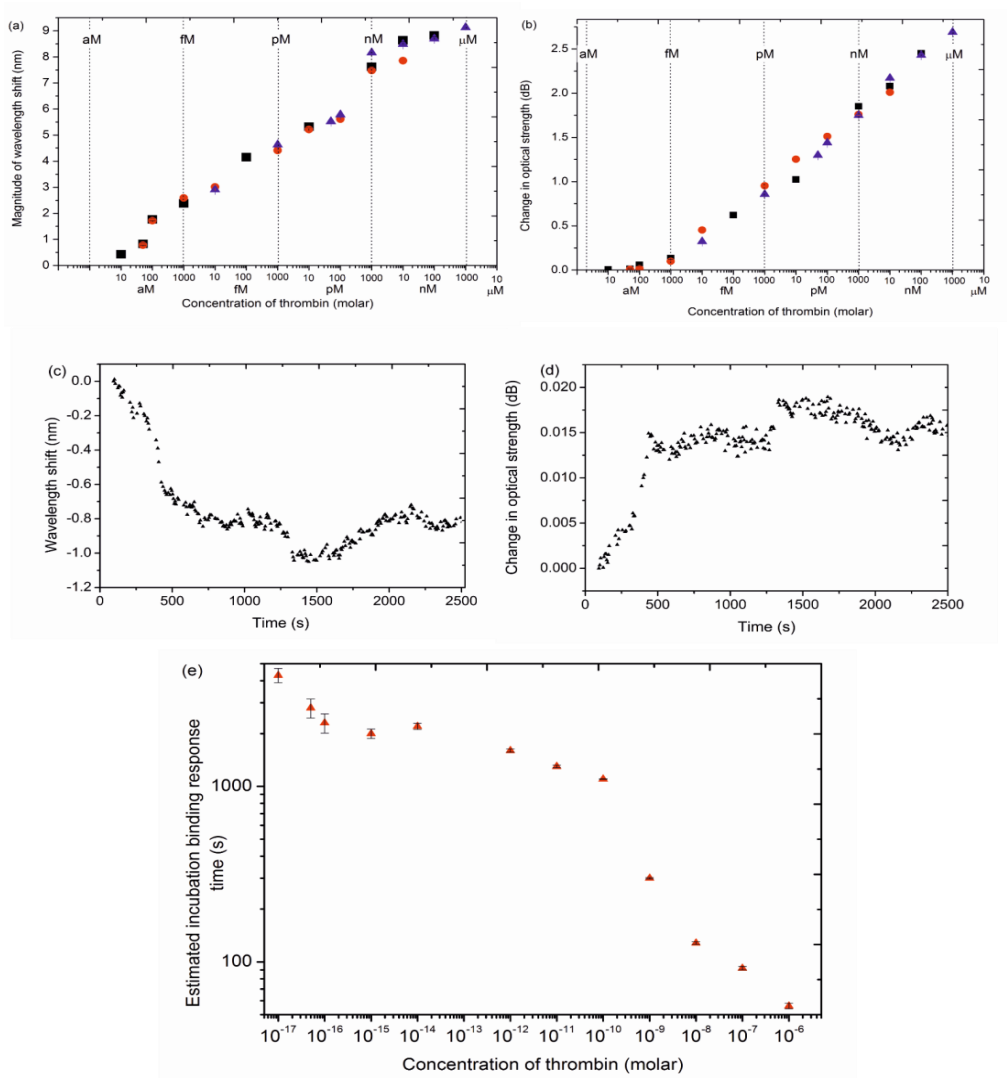

Fig. 7. Spectral sensitivity of aptamer-coated, static, multilayered SPR fibre devices (Au-SiO_2-Ge/fibre). (a) Change in optical coupling strength as a function of thrombin concentration. (b) Magnitude of wavelength change as a function of thrombin concentration. In parts a & b, ●, ▲, and ■ represent measurements made with three different devices. (c) Wavelength change and (d) Change in optical strength as a function of time after submersion in a static cell containing 50 aM thrombin (e) Estimation of the settling/incubation times of the binding reaction as a function of thrombin concentration.

To assist in the understanding of the device, concentration-response curves are shown in Fig. 8 for both change in wavelength and optical strength of the LSP resonance in the transmission spectra. We found that the devices had a saturation concentration of 36μM and produced a maximum wavelength shift of 9.6nm and 3.2dB change in optical strength. The Hill coefficient for equilibrium was determined for both the optical strength change and wavelength shift using the standard graphical approach [37] and yields $n_{H\text{intensity}} = 0.229$ and $n_{H\text{wavelength}} = 0.124$, respectively, indicating negatively cooperative binding; once the target molecule is attached to the binding enzyme/chemical, the affinity for other target molecules decreases.

Optics EXPRESS

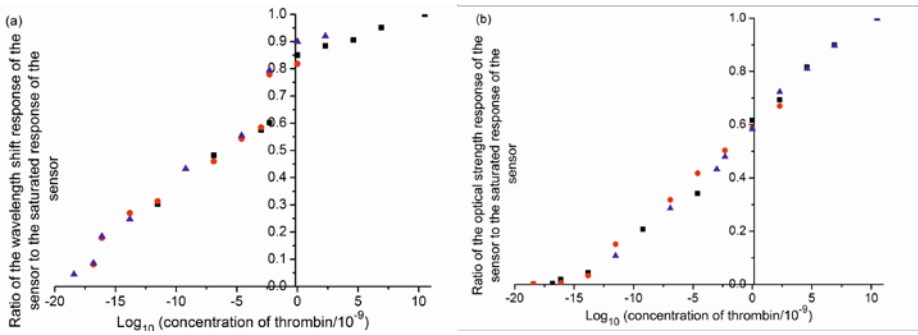

Fig. 8. The concentration-response curves of a (Au-SiO_2-Ge/fibre) device based upon (a) wavelength shift and (b) optical strength change.

Figure 8 yields half maximal effective concentration [38] (EC_{50}) of 14 pMolar and 96 pMolar for wavelength and optical strength, respectively. There are several approaches to estimate the limit of detection of this sensing platform. The detection limit can be estimated from the response with solutions at concentrations of 50aM and 5aM of thrombin in buffer; these two solutions produced wavelength shifts of 0.83nm and 0.43nm, respectively. There is a further complication associated with the measurement errors due to the increasing stochastic nature of the response of the system at these ultra-low concentrations, which can produce misleading results. A second approach is to use the EC_{10} value to yield an estimate of detection [38] using $EC_A = \left(A/(100-A) \right)^{-n_H} EC_{50}$, where A is the desired effective concentration and n_H is the Hill coefficient (determined experimentally). Thus the EC_{10} point is 96aM and 68fM for wavelength and optical strength, respectively. We expect this difference due to the fact that the physical mechanism that governs the coupling strength to the surface plasmon is different to that involved in the phase matching condition [13, 15, 17, 22] leading to different concentration-response curves.

Furthermore, another performance attribute of interest is the surface coverage resolution, which is the minimum identifiable valid change of molecular mass captured by the recognition molecule. The coverage can be defined [39] as $\sigma_\Gamma = \sigma_N h / \left(\Delta\lambda/\Delta n \right) \cdot \left(\Delta n/\Delta c \right)$ where σ_N is the associated noise within the result (0.24nm), h is the thickness of the layer that has the refractive index change associated with the aptamer molecule (assumed here to be of the order of the size of the thrombin molecule ~5nm) and $\Delta n/\Delta c$ is the volume refractive index increment of the molecular concentration, estimated to be about 0.18 cm^3/g (DNA or BSA [39, 40]) leading to 0.2pg/mm^2. This result again is amongst the highest from an optical sensing platforms reported in the literature [22–25, 41].

Detection limits of the flow device were then examined. The binding flow experiments were performed using thrombin in 0.6 mM (4.5% w/v) bovine serum albumin (BSA) / 50 mM Tris-HCl pH 7.4. As can be seen in Figs. 9(a) and 9(b), BSA alone gave a consistent response both in terms of wavelength and optical strength, even after regeneration. However, detection of 10 nM thrombin in the presence of 4.5% (w/v) BSA is demonstrated far more clearly when examining wavelength shift, Fig. 9(a), circled in red, than when examining optical strength, Fig. 9(b), red circle. Higher sensitivity from observing wavelength shift is here more pronounced but nevertheless consistent with data observed in the static format, Fig. 7.

Optics EXPRESS

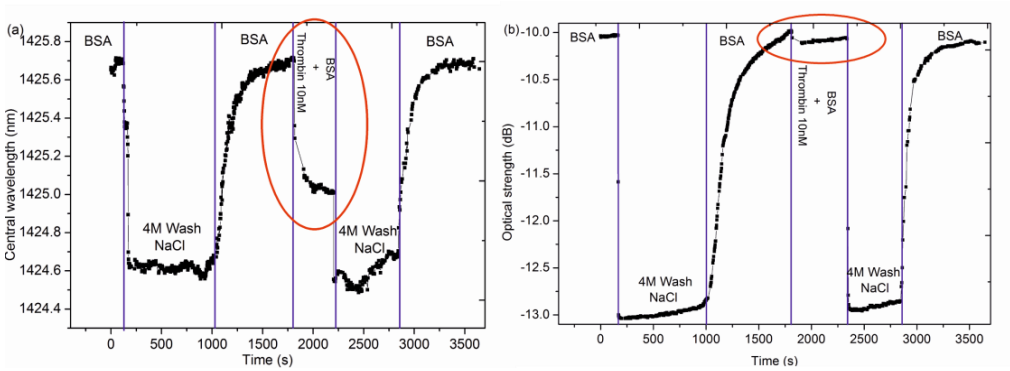

Fig. 9. The spectral response of an SPR (Au-SiO2-Ge/fibre) device with an immobilised thrombin aptamer on its surface in the sample flow cell format, with a constant flow rate of 5µl/min. Wavelength shift (a) and change in the optical strength (b) as a function of time. The sensor was initially washed with a 4.5% (w/v) BSA in Tris-HCl pH 7.4, then regenerated with 4 M NaCl, followed by second BSA wash. Thrombin (10 nM) in a 4.5% (w/v) BSA in Tris-HCl pH 7.4 was introduced at 1800 s, which was followed by another regeneration in 4 M NaCl and a final BSA wash.

One of the benefits of using an aptamer as the detecting molecule is that as single stranded DNA, it can also bind to its reverse complement. We therefore decided to examine both the specificity and sensitivity of the aptamer in the flow cell by examining the interaction with both complementary and non-complementary DNA sequences [30]. Figure 10 demonstrates ready detection of complementary DNA at a 100 pM concentration, with no detectable signal generated by a non-complementary sequence of similar length.

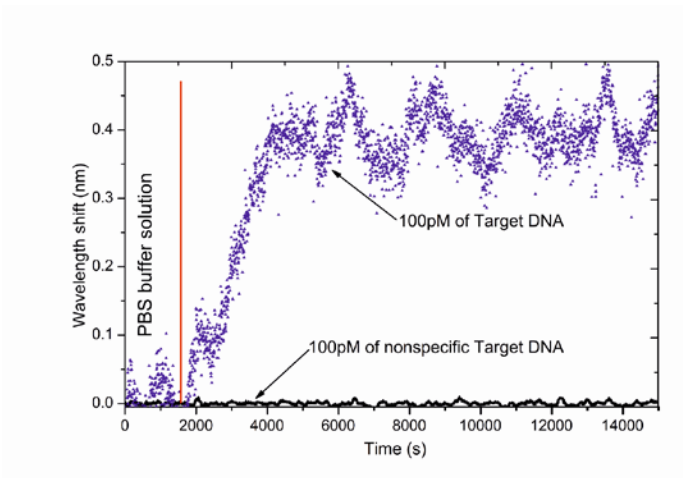

Fig. 10. Detection of hybridization between the DNA probe and both complementary and non-complementary single-stranded DNA sequences. The flow rate was 5 µl/min. The cell was first washed with buffer (300 mM NaCl, 20 mM Na_2HPO_4, 0.1 mM EDTA, 0.05% TWEEN® 20, pH 7.4). Non-complementary DNA was then introduced in the same buffer solution, followed by another buffer wash and then introduction of 100 pM complementary DNA, again in the same buffer.

4. Discussion

Inspecting all the experimental results including the examples shown in Figs. 4 and 5 over the range of concentrations used of thrombin and estimating their incubation times for each experiment, we observe times that are significantly smaller than the times predicted by conventional models based upon diffusion-limited capture for equilibrium reactions [40].

Optics EXPRESS

There is preceding literature that addresses this discrepancy [42–44]; the classical approach of modeling yields the mean incubation time, whilst experimental observations reveal the minimum detectable incubation time. It has been shown [43–45] for any sensor that the fundamental limit of detection for concentration under sufficiently long incubation times in a diffusion limited regime is given by a scaling relationship $\rho_0 t_{avg}^{M_D} \sim k_D$, where t_{avg} is the average or mean incubation time of the reaction, ρ_0 is the initial concentration, M_D and k_D are sensor-dimensionality dependent constants. These two constants have been studied [42] for various surface morphologies and for a nanowire geometry M_D ~1 and $k_D = \frac{N_s a_0}{D}$, where N_s is the minimum number of molecules needed to be captured for detection, D is the diffusion coefficient of the molecules and a_0 is the radius of the nanowires which in our case is about 30nm. Considering the conventional diffusion limit for an equilibrium, the diffusion coefficient can be calculated using the approach given in the literature [44]. We obtain a k_D value of ~8.091×10^{-10} leading to 8.091×10^7 s for the average incubation time of the reaction with a concentration of 10 aM for a volume of $1mm^3$ (approximately 30000 molecules of thrombin), which is approaching *937 days*.

Furthermore, at approximately 100 pico-molar concentrations there appears to be a distinct demarcation between the conventional equilibrium kinetic behaviour and a more stochastic kinetic nature. This can be seen by making a comparison of the general temporal response of the binding reaction for solutions with thrombin concentrations of 100nM and 100pM shown in Figs. 6(c) and 6(d). The response of the optical system to 100pM concentration solution starts to show fluctuations from a typical equilibrium time response, with more pronounced examples being shown in Figs. 7(c) and 7(d). This may be expected considering that the target thrombin molecule numbers are small in the volume of solution, and thus individual molecules can be considered to be acting independently from other thrombin molecules.

Assuming that the red wavelength shift in Fig. 6(a) is due to buffer ingression into the aptamer coating we can estimate the spectral and intensity sensitivity of the SPR device from Fig. 6(b). By working to the intensity detection limit associated with this interrogation scheme (0.1dB) and using linear regression with the experimental data, the following empirical relationships for strength and wavelength change with concentration were obtained: $\Delta I(dB) = 0.26\ln(Con_{cen}) + 1.82$ and $\Delta\lambda(nm) = 0.83\ln(Con_{cen}) + 7.15$, where Con_{cen} is the molar concentration of thrombin. These formulae permit the estimation of a minimum detectable concentration of thrombin in the buffer solution, which is approximately 5 aM; this was confirmed using thrombin concentrations down to 5aM, where no spectral changes were observed experimentally. The caveat here is that we are assuming the device has the same logarithmic spectral behaviour found at higher concentrations at the lower concentrations down to the limit of detection.

Comparing these results with those given in [46] (detection limits in the order of 1nM), this SPR device shows excellent detection sensitivity. Using the above data and the pseudo first-order kinetics approximation for the reaction of the aptamer and the thrombin, we estimated the association rate constant and the dissociation rate constant to be $1.06 \times 10^6 \pm 0.05 \times 10^6$ $M^{-1}s^{-1}$ and 0.24 ± 0.03 s^{-1} respectively, which leads to an equilibrium (association) constant of $4.28 \times 10^6 \pm 0.07 \times 10^6$ M^{-1}. These results compare well with the rate constant given in the literature [47–50] at similar concentrations. By comparison with our system, other approaches that make use of enhancement techniques may be compromised by the inclusion of additional particles to support the plasmons [22]. Similarly the approaches that make use of labelling also require the presence of additional species, e.g. fluorophores [1].

The demonstration of thrombin detection in a 4.5% (w/v) BSA protein in binding buffer (50mM Tris 140mM NaCl 1mM $MgCl_2$) pH 7.4, given in Fig. 9 shows that BSA protein can

Optics EXPRESS

be distinguished from the thrombin and that the thrombin has preferential interaction over the BSA. The authors do acknowledge that in real world applications using blood plasma there are a large number of other complex compounds and proteins present and nonspecific co-present binding cannot at this stage be ruled out. Nevertheless this particular test with 4.5% (w/v) BSA with thrombin is a step closer to the composition of blood, where the albumin (in humans it is human serum albumin) is the most common protein. Due to the concentration levels of the albumin protein it may adhere to the surface of the sensor and thus act as a blocker for the attachment of the thrombin to the aptamer. The detection limit of thrombin in the BSA solution was obtained by determining the experimentally observed wavelength shift as a function of thrombin concentration and using the spectral resolution of the resonance itself [33]; this yielded approximately 0.1nM, which is in the initial concentration range in the lag time of the typical human thrombin generation curve [51–56] (HTGC) resulting from samples taken from patients. Furthermore these sensing devices can also be used over the complete concentration range of a HTGC; at the peak thrombin level and through the endogenous thrombin potential [52–54].

The average time interval between successive measurements varied for each experiment from 2 seconds to 6 seconds. The OSA covered an extended spectral range to observe as much of the transmission feature of the sensing platform as possible, up to approximately 400nm. The measurement time can be dramatically reduced to sub-second if required by reducing the spectral scanning range. The 3dB bandwidth of the localised surface plasmon excitation in the transmission spectrum varies from 80 nm to 200 nm (typical transmission spectrum from a device is shown in Fig. 5(d)). The interrogation scheme could be changed to other techniques that have higher data acquisition rates. For existing biosensing systems, the response time becomes excessively long for femtomolar and attomolar concentrations, ranging upwards from 300 seconds to as much as 10^5 seconds [19]. Response time is important for a significant number of label-free clinical applications [29,46] and these times mean that the monitoring of real-time kinetics is not possible. The detection technique presented here yields continuous meaningful experimental data on an acquisition rate of approximately a second or less at femtomolar and attomolar concentrations and thus true binding kinetic data can be obtained.

We can compare our performance against other thrombin sensing technologies, for example the Biacore system. That has a detection limit in concentration of around 10 pM [54], which is six orders of magnitude less sensitive than ours and yet has higher sensitivity compared to approaches such as electrochemical detection, where the detection limit is approximately 0.4nM [56], or other methods that employ a surface plasmon resonance, which yield 5nM [45]. Recently an SPR device with an enzymatic amplification approach [48] yielded a limit of 500 fM, this still represents several orders poorer resolution than the SPR device reported here. There are several approaches to the detection of thrombin with aptamers and most of these techniques have a limit of detection of approximately 1 to 10nM [49]; this again is significantly less sensitive. Secondly comparing this scheme of detection to the conventional methods of measuring thrombin and associated coagulants: instruments with similar performance are financially expensive and not compatible with remote, real-time operation. The presented scheme has the potential to be made relatively cheap and compact whilst still offering similar or better performance to the more conventional systems [55]. It must be stated that some of the detection schemes use small solution volumes, comparable to the volume used in this series of experiments, thus it's reasonable to quote the total number of molecules/particles that are being detected, which is 30000. This may appear to be a large number compared to other schemes but a better comparison is the sensing coverage [34] for this particular molecule (thrombin), which is estimated be to 0.2pg/mm^2 that is amongst the highest from an optical sensing platforms reported in the literature [23–25, 39].

In conclusion, we have demonstrated a new opto-bio-sensing platform based upon aptamers immobilised onto an optical sensing structure that utilises infrared localised surface

Optics EXPRESS

plasmons to provide a detection limit of a few attomolar concentrations of thrombin in a sodium phosphate buffer solution. This significantly outperforms other types of sensing platforms including fibre optic, surface plasmon or electrochemical thrombin sensors by four orders of magnitude. Our demonstrated approach offers advantages, for example the ability to evaluate variations in the picomolar range, which is inaccessible with classical techniques. In addition the performance of the device in the presence of non-specific protein provides an early indication that the sensitivity and specificity of the device may be maintained in a realistic environment.

Moreover, we may compare this optical sensing scheme to other fibre optical sensing methods, where the best reported performance to date is limited to detection levels of 500 fM [48]. This limit of a few hundred fM has been echoed in a recent review paper [48]. Making a comparison to the other detection techniques [56, 57] the opto-bio-sensing platform offers the opportunity to collect real-time data for kinetic studies at ultra-low concentrations in the femtomolar and attomolar ranges. The range of biological and chemical molecules for which high affinity aptamers have been developed is extensive and aptamer development continues apace. The successful employment of the well characterised 15 mer thrombin binding aptamer to our sensing device suggests our technology also has the potential to detect ultra-low concentrations of other chemicals, taking advantage of the so-called “lock-and-key” relationship between aptamers and their binding partners [49]. Furthermore, the chemical selectivity test was performed with another compound, a DNA probe, which provided evidence that this optical platform reflects the affinity of the binding molecule to the target molecule.

The combination of this next generation localised surface plasmon sensing scheme with aptameric functionalised coatings offers great potential for remote sensing [55], providing as it does both high sensitivity and selectivity, coupled with a small physical footprint and low loss fibre connecting leads. In this regard the environmental application to remote sensing arrays for the detection of ultra-low concentrations of harmful substances is quite apparent. For example, our system has the potential to readily target estrogenic compounds, herbicides, pesticides, and industrial by-products that persist especially in the agricultural environment, which can cause infertility, deformed reproductive organs and other biological defects in extreme cases [50].

Funding

This work was financially supported by grants EP/J010413 and EP/J010391 for Aston University and the University of Plymouth from the UK Engineering and Physical Sciences Research Council. To access the data underlying this publication, please contact researchdata@aston.ac.uk., see, http://doi.org/10.17036/researchdata.aston.ac.uk.00000179.

Acknowledgments

Firstly the authors would like to give special mention and a heartfelt thankyou to the late Professor Marco Mascini (who passed away suddenly and unexpectedly during the course of this work). Without his professional and personal generosity this work would not have been started and progressed to this point. Also we would like acknowledge and thank the late Mr. Mark A. Turner for his help and efforts in designing and fabricating the flow cells. Each of the authors contributed as following: T. A. and I. B. developed the original plasmonic concept. T.A. modelled, designed and performed experiments, analysed the data for the plasmonic devices. T.A., C.M., R.N., S. R. fabricated the plasmonic devices. S. T., S.M. and M. M. developed and adhered the aptamer coatings to plasmonic devices. D. N. and A. P. prepared biological compounds and solutions for experiment, designed, performed experiments. T. A., K.K. developed the explanation for sensor behaviour and performed experiments. The manuscript was written by T.A., A.V. H., D. N., K.K., D.J.W., R. N. and P.C. All authors discussed the results and commented on the manuscript.